Chemical Engineering Journal 454 (2023) 140239

Contents lists available at ScienceDirect

Chemical Engineering Journal

journal homepage: www.elsevier.com/locate/cej

Sequential hydrothermal carbonization and CO_2 gasification of sewage sludge for improved syngas production with mitigated emissions of NO_x precursors

Weiming Huang [a], Ruichi Zhang [b], Apostolos Giannis [c], Chuanhao Li [a,*], Chao He [b,*]

[a] School of Environmental Science and Engineering, Sun Yat-sen University, Guangzhou 510006, China
[b] Faculty of Engineering and Natural Sciences, Tampere University, Tampere, Finland
[c] School of Environmental Engineering, Technical University of Crete, Greece

ARTICLE INFO

Keywords:
Low temperature pretreatment
CaO catalysis
Tar cracking
Nitrogen transformation
Syngas quality
Gasification efficiency

ABSTRACT

Due to high moisture and protein contents in sewage sludge (SS), conventional thermal treatment of SS is energy-intensive and a large amount of harmful nitrogen-containing gases are emitted. In this study, a sequential hydrothermal carbonization (HTC) and CO_2 gasification system has been proposed to effectively improve the gasification efficiency and considerably reduce the emissions of NO_x precursors (i.e., NH_3 and HCN) in SS treatment. Yield and quality of syngas were comprehensively investigated during CO_2 gasification in terms of various temperatures with different dosages of CaO additive in HTC, and varied reaction temperature and CO_2 percentage in gasification process. On the whole, CO_2 gasification of SS derived hydrochar (HC) demonstrated obvious reduction of tar formation from 10.9 to 6.8 % and enhancement of calorific value of formed syngas from 14.1 to 15.7 MJ/Nm^3. Production of NO_x precursors was greatly reduced due to formed non-active quaternary-N in HC, while HTC with CaO favored the mitigated NO_x precursors in syngas owing to enriched pyrrole-N and quaternary-N therein. Catalytic tar decomposition and Boudouard reaction in CO_2 gasification were responsible for the distinct reduction of tar formation, and notable increase of carbon conversion ratio and syngas yield. Although facilitated catalytic gasification in CO_2 atmosphere can maximize syngas yield, lower portion of CO_2 (ca. 20 %) was more beneficial to drastically mitigate emissions of NO_x precursors, especially the reinforced transformation of NH_3 to N_2. The fundamental knowledge could ultimately help to achieve significant abatement of NO_x precursors during CO_2 gasification for improved syngas production.

1. Introduction

Rapid urbanization has caused remarkably increasing generation of sewage sludge (SS) from wastewater treatment plants (WWTPs). However, SS is also considered as source of fuels and resource because of abundant organic compounds (e.g., polysaccharides, proteins and lipids) and nutrients (e.g., nitrogen and phosphorus) [1,2]. Currently, landfilling, composting, and thermochemical conversion (e.g., incineration, pyrolysis and gasification) are mainly applied for SS treatment [3,4]. Among them, gasification has attracted increasing attention due to its capability in converting biomass and wastes into more efficient fuel gas [5,6]. Nevertheless, the relatively high nitrogen content in SS (2.4–9 wt %) impedes the wide application of gasification [7–9] because the produced syngas contains a large amount of nitrogen-containing gases, such as NH_3 and HCN. These gases can be transformed into the harmful NO_x after combustion [10]. Previous studies have found that 30–55 % of nitrogen in raw materials (i.e., bean straw and rice straw) could be transformed into *N*-containing gaseous pollutants during the pyrolysis process [11,12]. Hence, it is crucial to apply an effective pretreatment step to reduce the nitrogen content in the feedstock, which benefits the reduction of *N*-containing gaseous contaminants in the subsequent gasification stage. To date, hydrothermal carbonization (HTC) has been proved and widely applied as an effective pretreatment process due to high nitrogen removal efficiency and improved fuel quality [13–15]. Because the Ca-based additive accelerated the formation of free radicals and improved alkalinity of reaction system during HTC, calcium oxide (CaO) can synergize with hydrothermal reactions to remove nitrogen more efficiently [9,16,17]. Apart from the removal of *N*-containing

* Corresponding authors.
E-mail addresses: lichuanh3@mail.sysu.edu.cn (C. Li), chao.he@tuni.fi (C. He).

https://doi.org/10.1016/j.cej.2022.140239
Received 2 September 2022; Received in revised form 19 October 2022; Accepted 3 November 2022
Available online 9 November 2022

compounds before fuel utilization, stable *N*-containing compounds are vital for the operation of power plant. Quaternary-N is a more stable nitrogen functionality, which can cut off the desirable process for the formation of NH_3 in gasification/pyrolysis [8]. The remaining amine-N is converted into pyrrole-N, pyridine-N and quaternary-N in solid product after HTC [14]. It has been reported that CaO additive could favor transformation of protein-N to nitrile-N and pyridine-N in the higher HTC temperature condition (380 ℃) [9], thereby improving the stability of nitrogen in HC. However, higher HTC temperature will increase the cost and weaken the function of CaO. Therefore, it is essential to investigate the effect of CaO additive on the evolution of nitrogen functionalities under lower hydrothermal temperatures (less than220 ℃).

Actually, the use of hydrochar (HC) as feedstock in gasification process could not only decrease the activation energy of feedstock [16,18] and inhibit tar formation [19], but also improve the yield and calorific value of syngas [20,21]. The majority of previous studies are related to the gasification of biowaste using steam as the gasification agent as it favors the production of hydrogen-rich gas [22–24]. However, the generation of high-temperature steam during gasification would not only decrease the overall thermal utilization efficiency, but also increase the operational cost resulting from the huge energy consumption, which is not conducive to the efficient and sustainable development of the system [25]. Recently, carbon dioxide (CO_2) has become an alternative gasification agent attributed to enhanced thermal efficiency and reduced tar production [17,26]. Comparing with steam, introducing CO_2 generally increases CO content and enhances carbon conversion due to the reaction of CO_2 and carbon during gasification system [27,28]. Besides, CO_2 could greatly increase the gas production, carbon conversion and cold gas efficiency [27], indicating that CO_2 plays a significant role as gasification agent in biomass gasification process. Nonetheless, these studies mainly utilized lignocellulosic biowaste (e.g., rice straw or wood) as feedstocks, limited research has been performed on CO_2 gasification of SS. Moreover, most CO_2 gasification experiments of biowaste have been carried out under a CO_2 content of 10–30 %. However, the effect of CO_2 content on the gasification performance and yield of NO_x precursors during CO_2 gasification of SS is not well known. Hence, it is imperative to explore the CO_2 gasification characteristic of SS and the effect of CO_2 content on the syngas quality, tar production and emissions of NO_x precursors.

Exploration of the conversion pathways of nitrogenous compounds during CO_2 gasification is a necessity to identify the reduction mechanism of NH_3 and HCN. There are few studies on the transformation and conversion of nitrogen during CO_2 gasification of SS, which is essential for the reduction of NO_x precursors and the quality of syngas. It has been reported that introducing CO_2 as gasification agent has a vital effect on the emissions of *N*-containing gas. In addition, CO_2 could react with char and promote the release of volatile-N to form NO during the co-pyrolysis/gasification of SS and corn straw under CO_2/Ar or O_2/Ar atmosphere [29], indicating that different atmosphere could affect the pathway of fuel-N transformation.

Therefore, this study aims to explore the effect of CaO on the transformation of nitrogen functionalities in low temperature HTC process, and the effect of CO_2 on the gasification performance as well as emission characteristics of nitrogen-containing gases. Better understanding will be obtained regarding the reduction mechanism of NO_x precursors during CO_2 gasification of SS. Specifically, this study will reveal the nitrogen transformation pathways during CO_2 gasification coupled with HTC pretreatment. In particular, gasification performance will be comprehensively evaluated in terms of yield and quality of syngas, release characteristics of NH_3 and HCN, and the evolution of nitrogen in char and tar. Eventually, insightful knowledge will be acquired to manipulate gasification efficiency with mitigated NO_x precursors.

2. Materials and methods

2.1. Materials

Dewatered SS was collected from a WWTP in Guangzhou, China. Prior to analysis, the SS was subjected to drying, milling, sieving to fine particles less than 200 μm, followed by storage in desiccator. Table 1 summarizes the physicochemical properties of SS.

2.2. Experimental

2.2.1. HTC process

HTC experiments were performed in a 250 mL autoclave (Hastelloy C276, HT-250JOC, HTLAB, Shanghai Huo-Tong Experimental Instrument Co., ltd.). Briefly, in each experiment, SS with 5 % solid content was used by mixing 4 g SS with 80 mL of deionized water in the reaction vessel. In another set of experiments, different dosages of CaO (e.g., 73.2, 109.1, 147.0 mg corresponding to Ca/C (C in SS) molar ratio of 0.05, 0.075, 0.1, respectively), were added during HTC process. The vessel was then sealed and purged with N_2 for 10 min to remove residual air. Afterwards, the reactor was heated to a pre-set temperature (i.e., 180, 200 and 220 ℃). The reaction time and stirring speed were set at 30 min and 180 rpm, respectively. The reactor was quickly quenched to room temperature in a water bath after the reaction was completed. The hydrothermal slurry was filtered through 0.45 μm PTFE membrane to obtain the filtrate and solid fraction that was designated as hydrochar (HC). The aqueous phase was stored in a 4 ℃ refrigerator before measurements of *N*-containing substances, including total dissolved nitrogen (TDN), ammonia-N (NH_4^+-N) and nitrate-N (NO_3^--N). The HC was oven dried at 105 ℃ for 24 h and labeled as HCX_1-X_2, where X_1 and X_2 stand for hydrothermal temperature (i.e., 180, 200 and 220 ℃) and Ca/C molar ratio (i.e., 0.05, 0.075 and 0.1), respectively. The X_2 was not labeled when there was no CaO additive.

2.2.2. CO_2 gasification

CO_2 gasification experiments were performed in a vertical tube furnace gasification set-up which was mainly composed of a feeding cylindrical crucible, a fixed-bed reactor, an electric heater, and mass flow controllers. The schematic diagram of the reaction set-up is shown in Fig. 1. Approximately 500 mg of SS or HC was placed in the crucible in each experiment run. The gas flow rate was set at 300 mL/min when using 100 % N_2 or CO_2 as gasification agent. Under mixed gasification agent of 20 %CO_2 and 80 %N_2 (namely $20CO_2 80CO_2$), the flow rate was set to 60 and 240 mL/min for CO_2 and N_2, respectively. During the experiments, the heating rate of the furnace was set at 10 ℃/min. When the reactor reached the desired temperature (i.e., 700, 800 and 900 ℃) and gas flow (300 mL/min), the electric heater was moved down until the heating zone was at the same height as the feeding quartz, and a reaction time of 30 min was maintained. The produced syngas sequentially passed through the following collection units: 1) tar condensation unit filled with isopropanol; 2) NO_x precursors absorbing unit (0.1 mol/L H_2SO_4 for NH_3 and 0.2 mol/L NaOH for HCN); and 3) collection gas bag. After each experimental run, tar was collected using a rotary evaporator, and then the collected tar was weighed and re-dissolved for further analysis using gas chromatography-mass spectrometry (GC–MS). Solid residues were collected, weighed and stored for further analysis. Each experiment run was carried out in duplicate under identical condition.

2.3. Analytical methodologies

2.3.1. Characterization of solid fraction

The elemental composition of solid products (SS, HC, solid residue (SR)) was determined by CHNS analyzer (Elemental vario EL, Germany). The proximate analysis (ash content and volatile matter (VM)) was measured by a muffle furnace in accordance with the China National

Table 1
Physicochemical properties of sewage sludge.

Ultimate analysis (wt.%, db)					Proximate analysis (wt.%, db)			Fuel ratio	HHV (MJ/kg)
C	H	N	S	O [a]	Ash	VM	FC	FC/VM	
25.74±0.15	3.99±0.01	4.29±0.01	0.68±0.10	18.73±0.05	46.57±0.16	46.21±0.21	7.22±0.24	0.16	10.77
Ash analysis (expressed as wt.% of metal oxides)									
SiO_2	Al_2O_3	Fe_2O_3	CaO	MgO	P_2O_5	K_2O			
39.90	29.10	5.50	3.92	3.07	12.10	2.77			

Notes:
db, dry basis; VM: volatile matter; FC: fixed carbon; HHV: higher heating value.
[a] Calculated by difference.

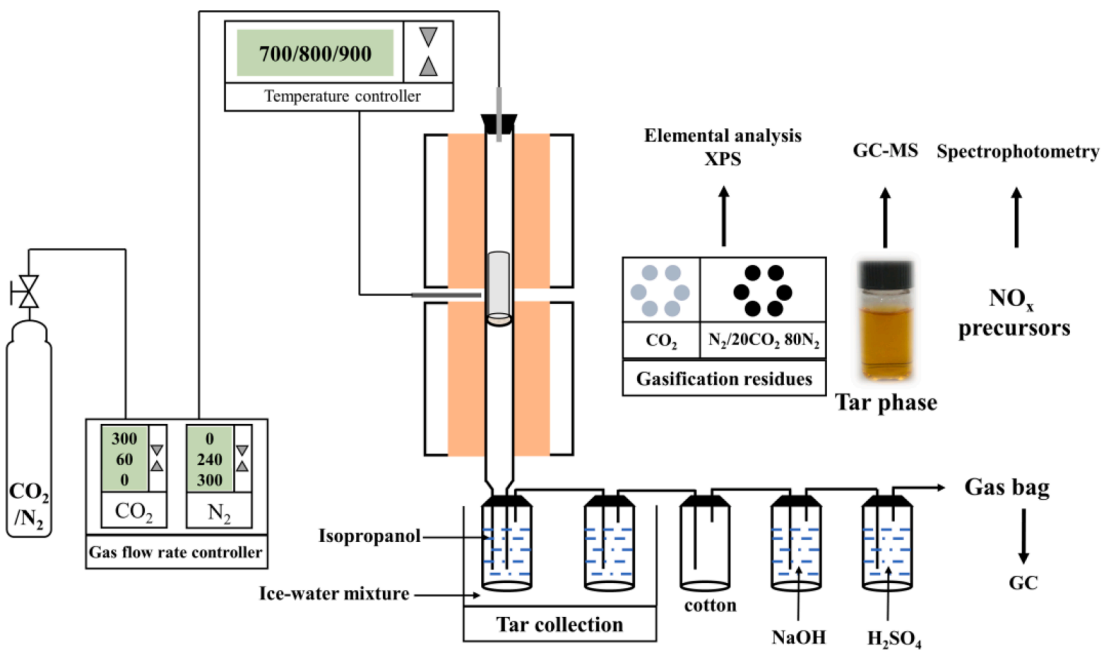

Fig. 1. Schematic diagram of experimental set-up for CO_2 gasification.

Standard (GB/T 28731–2012). The proportion of oxygen and fixed carbon (FC) were calculated by difference (Eqs. (1) and (2)). Higher heating value (HHV) of feedstock was estimated using Eq. (3) [17]. The composition of metal oxides in ash was determined by X-ray Fluorescence (XRF, XRF-1800, SHIMADZU).

$$FC\ (\%) = 100\ \% - Ash - VM \tag{1}$$

$$O = 100\ \% - C - H - N - S - Ash \tag{2}$$

$$HHV = 0.3491 \times C + 1.1783 \times H + 0.1005 \times S - 0.1034 \times O - 0.0151 \times N - 0.0211 \times Ash \tag{3}$$

where C, H, S, O, N, FC, VM and Ash represent the weight percentage of C, H, S, O, N, FC, VM and Ash in the solid samples, respectively.

The crystal phase of SS was measured by X-ray diffraction (XRD, Ultima IV, Japan) patterns over a 2θ ranged from 5° to 80°. Surface functional groups of solid samples were determined by Fourier transform infrared (FT-IR) spectroscopy (Nicolet iS10, Thermo Fisher Scientific, USA). X-ray photoelectron spectroscopy (XPS) was carried out on a Thermo Fisher Scientific ESCALAB 250 spectrometer equipped with Al Kα X-ray radiation source (hv = 1486.6 eV). N 1 s XPS spectra of solid powders were analyzed under identical conditions. The charge calibration was made by setting the binding energy of adventitious carbon to 284.8 eV. The gasification performance of SS and HC was conducted by a thermogravimetric analyzer (METTLER TOLEDO TGA/DSC 3 +) under the presence of N_2 or CO_2 atmosphere. In each test, approximately 10 mg of sample was loaded and heated from 30 to 1050 ℃ at a heating rate of 10 ℃/min with a gas flow rate of 50 mL/min under atmospheric pressure.

2.3.2. Characterization of aqueous phase and tar

Total dissolved nitrogen (TDN) and ammonia-N (NH_4^+-N) in the aqueous phase from HTC were measured using HACH DR 3900 spectrophotometer with HACH total nitrogen (TN) and NH_4^+-N test kit. Nitrate-N (NO_3^--N) was determined following the standard procedures of China National Standard (HJ/T 346–2007). The amount of organic nitrogen was calculated by the difference of TDN and inorganic nitrogen (NH_4^+-N and NO_3^--N). Main organic components in formed tars were analyzed by GC–MS (Agilent Technologies, USA) equipped with a chromatographic column (HP-5MS, 30 m × 0.25 mm × 0.25 μm).

2.3.3. Analysis of gases

Collected gases from gasification were analyzed by a gas chromatograph (GC, SHIMADZU, GC-2014C) equipped with a thermal conductivity detector (TCD) and flame ionization detector (FID) to quantify the amounts of H_2, CO, and CH_4 in the gas mixture. The lower heating value of gaseous products (LHV_{gas}, MJ/Nm^3) was estimated according to Eq. (4) [20]. Gas yield was normalized based on carbon content as described in Eq. (5), where H_2, CO and CH_4 represent proportion of H_2, CO and CH_4 in the gas mixture, respectively. Gas $production_C$ and Gas production are the gas production normalized by carbon content and the initial gas production measured by GC, respectively; $m_{feedstock\text{-}C}$ is the carbon content in the feedstock, which is calculated through the mass weight

and nitrogen proportion derived from ultimate analysis.

$$LHV_{gas} = 10.8 \times H_2 + 12.6 \times CO + 35.8 \times CH_4 \quad (4)$$

$$\text{Gas yield} = \text{Gas production} / m_{feedstock\text{-}C} \quad (5)$$

NH_3 and HCN were absorbed in the H_2SO_4 and NaOH solutions to form NH_4^+ and CN^- that could be quantified using the standard procedures of China National Standards HJ 535–2009 and HJ 484–2009, respectively. Yields of NH_3-N and HCN-N were calculated according to the ion concentration and nitrogen content in the feedstock used for gasification using Eqs. (6) and (7) [8], where $M_{NH3\text{-}N}$ and $M_{HCN\text{-}N}$ are the mass production of NH_3-N and HCN-N, respectively, C_1 and C_2 are the concentration of NH_4^+ and CN^-, respectively, in the absorbed solutions; V_1 and V_2 are the volumes of the corresponding absorbed solutions; $m_{feedstock\text{-}N}$ is the nitrogen content in the feedstock, which is calculated through the mass weight and nitrogen proportion derived from ultimate analysis.

$$M_{NH3\text{-}N} = [(C_1 \cdot V_1 \cdot 14.01) / 18.04] / m_{feedstock\text{-}N} \quad (6)$$

$$M_{HCN\text{-}N} = [(C_2 \cdot V_2 \cdot 14.01) / 26.02] / m_{feedstock\text{-}N} \quad (7)$$

2.4. Gasification performance evaluation

Carbon conversion ratio (CCR) which describes the amount of converted carbon during the process can be calculated through Eq. (8) [17].

$$CCR = 1 - \frac{\text{carbon content in the solid residue } (\%) \times \text{mass of solid residue } (g)}{\text{carbon content in the feedstock } (\%) \times \text{mass of feedstock } (g)} \quad (8)$$

3. Results and discussion

3.1. Effect of HTC on fuel characteristics of hydrochar

3.1.1. Physicochemical properties of HC

Hydrothermal treatment of SS can generate hydrochar (HC), aqueous fraction and gases. Generally, HC yield was in the range of 65.4–74.1 % (Fig. 2). In the absence of CaO, HC yield decreased gradually from 70.4 % to 65.4 % as the temperature increased from 180 to 220 ℃. The higher HTC temperature accelerated hydrolysis and dehydration of SS, and favored decomposition of the organic matters (e.g., polysaccharides, proteins, etc.) into the liquid phase [30]. It was reported that the addition of CaO could catalyze the decomposition of organic matters in SS, thus resulting in a decreased HC yield [17,31]. However, in this study, the overall HC yield had an increasing trend with the increased Ca/C molar ratio. This was probably attributed to the formed $CaCO_3$ or $Ca(OH)_2$ in HC with the addition of CaO [9]. Moreover, CaO could facilitate the hydrolysis and deamination of proteins and carbohydrates contained in SS, thus resulting in increased amino acids concentrations and decreased sugar content in the aqueous phase. The accumulated amino acids could be re-transferred to the solid phase though polymerization and Maillard reactions [32]. The elemental and proximate analyses of HC are presented in Table 2. Lower N content in HC was observed compared to SS (Table 1), and the N content further decreased with the increased HTC temperature and CaO addition. This process is favorable as the production of NO_x precursors could be reduced in the subsequent gasification process [10].

The FT-IR spectra of SS and HC are shown in Fig. S1. There were no significant differences between SS and HC. The spectra of SS and HC showed obvious peaks of amide groups, including 3287 cm^{-1} (N—H stretching, amide II), 1640 cm^{-1} (C═O stretching, amide I) and 1523 cm^{-1} (N—H stretching, amide II) [14,30]. The intensity of N—H and C═O stretching decreased with the increased temperature and Ca/C molar ratio. The resulted indicated that higher temperature and the addition of Ca-based catalyst could decrease amide-N content by breaking peptide bonds (–CO-NH-). The peak at 1030 cm^{-1} was probably attributed to Si-O stretching, which revealed the presence of SiO_2 [33], which was also confirmed by XRD analysis (Fig. S2).

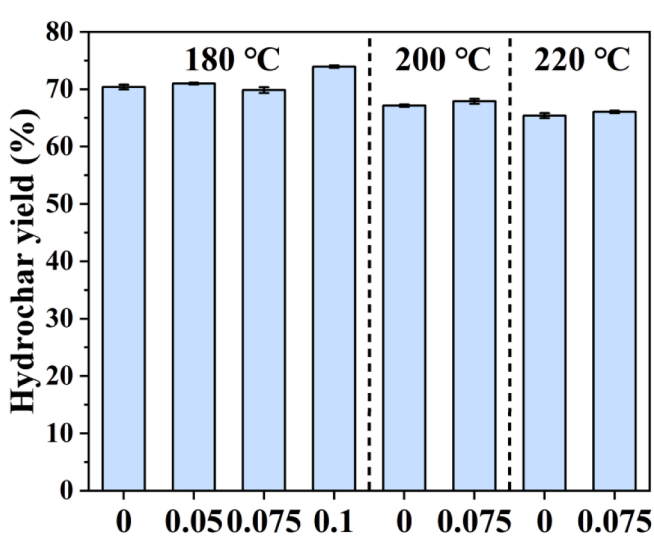

Fig. 2. Hydrochar yield in HTC under different reaction temperatures and Ca/C molar ratios.

3.1.2. Gasification of HC under CO_2

Effect of CaO on SS and HC during thermal decomposition under CO_2 atmosphere is shown in Fig. 3. All samples had three major stages of mass loss during the thermal process: VM decomposition (240–400 ℃), FC combustion (400–510 ℃) and gasification conversion (700–1050 ℃) [9,34]. The total mass loss of SS could reach 56.24 % when the temperature was increased to 975 ℃ (Fig. 3a). HTC pretreatment could decompose partial VM and increase the non-active ash content in HC, which resulted in a decrease in total mass loss. This effect was enhanced with the increased HTC temperature. The HTC pretreatment could also affect the decomposition temperature (Fig. 3b). It was found that HTC could increase the T_i (the initial VM decomposition temperature) from 333 ℃ (SS) to 363 ℃ (HC220), indicating that HTC could increase the stability of VM which needed higher energy to be decomposed. Similar result was observed in FC combustion stage, slightly increasing form 456 ℃ (SS) to 460 ℃ (HC220). In the gasification conversion stage, HTC pretreatment decreased the onset gasification temperature. The result revealed that HTC pretreatment could decrease the activation energy for gasification. Similar observation was reported by Zhuang et al. that HTC pretreatment temperature (180–240 ℃) could lower the activation energy for biowaste gasification [20].

Interestingly, compared with HC produced without CaO additive, the mass loss of HC with CaO additive was not significantly affected (Fig. 3c). These results suggested that CaO could further promote the decomposition of VM or FC combustion. The results of differential thermogravimetric (DTG) analysis could further confirm this hypothesis (Fig. 3d). In the first two stages (VM decomposition and FC combustion),

Table 2
Physicochemical characteristic of HCs.

Samples	Ultimate analysis (wt %, db)					Proximate analysis (wt%, db)			Fuel ratio	HHV (MJ/kg)
	C	H	N	S	O [a]	Ash	VM	FC	FC/VM	
HC180	18.67±0.47	3.20±0.17	2.06±0.05	ND [b]	12.88±0.04	63.19±0.64	32.30±1.05	4.51±0.41	0.14	7.59
HC200	17.09±0.08	2.95±0.11	1.67±0.01	ND	11.31±0.17	66.98±0.19	28.18±0.11	4.84±0.30	0.17	6.83
HC220	16.71±0.55	2.65±0.05	1.52±0.02	ND	10.09±0.14	69.03±0.11	26.28±0.01	4.69±0.11	0.18	6.43
HC180-0.005	18.02±0.12	3.29±0.05	1.73±0.02	ND	-	62.31±1.70	-	-	-	-
HC180-0.075	17.20±0.08	3.09±0.14	1.69±0.01	ND	-	62.46±0.68	-	-	-	-
HC180-0.1	18.35±0.15	3.39±0.12	1.81±0.02	ND	-	62.45±1.18	-	-	-	-
HC200-0.075	16.71±0.16	2.95±0.09	1.48±0.02	ND	-	67.75±0.23	-	-	-	-
HC220-0.075	15.51±0.13	2.54±0.07	1.36±0.01	ND	-	68.82±0.51	-	-	-	-

Notes:
db, dry basis; VM: volatile matter; FC: fixed carbon; HHV: higher heating value.
-: Not applicable. $CaCO_3$ could form via carbonization after adding CaO during HTC process. In ultimate analysis, decomposition of inorganic $CaCO_3$ affected accurate O calculation. In proximate analysis, $CaCO_3$ could be decomposed into CaO and CO_2 under high temperature, which would increase the content of VM and affect the whole proximate analysis calculation.
[a]Calculated by difference.
[b]ND, Not detected.

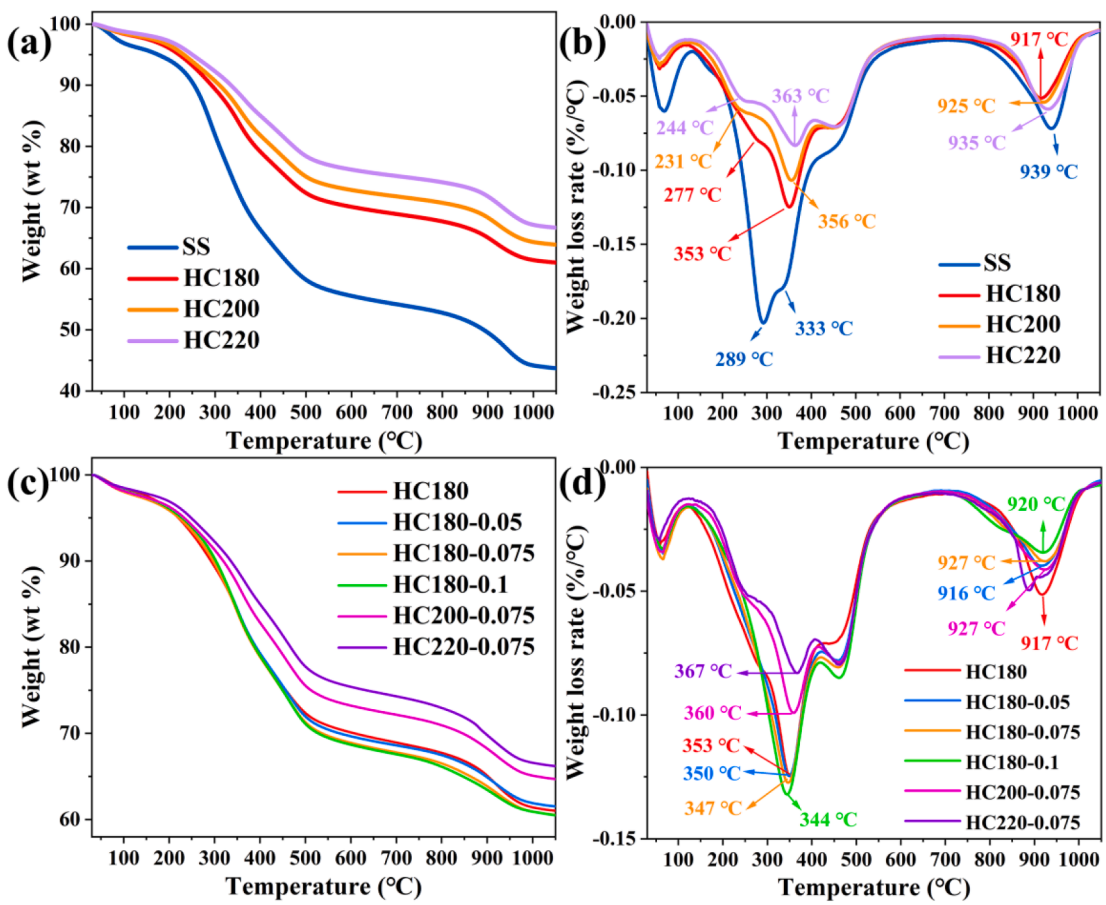

Fig. 3. Thermal decomposition profiles for SS and HC under CO_2 atmosphere: Effect of hydrothermal temperature on (a) TG and (b) DTG; Effect of different Ca/C molar ratios in HTC on (c) TG and (d) DTG.

addition of CaO for HC180 could improve the maximum mass loss rate, suggesting that CaO promoted the decomposition of VM and FC. Indeed, adding CaO could lower the T_i from 353 ℃ (HC180) to 344 ℃ (HC180-0.1) as presented in Fig. 3d, indicating that CaO could lower the required temperature of VM decomposition owing to catalytic reactions. The second peak around 450 ℃ became wider and more obvious for HC with CaO addition. It is assumed that this phenomenon could be related to the transformation of CaO to $Ca(OH)_2$ during HTC, and the additional decomposition of $Ca(OH)_2$ may extend the second range [9]. However, compared with HC180 or HC180-0.05, higher Ca/C molar ratio (e.g., HC180-0.075 and HC180-0.1) could shift to a higher temperature for the peak corresponding to the maximum conversion rate within gasification stage (Fig. 3d). These changes were ascribed to the improved aromaticity after adding CaO during HTC, which delayed the peak for gasification of HC [20].

Compared with SS and HC decomposition in N_2 atmosphere (Fig. S3), the most significant difference was the gasification stage. For SS, mass loss was not significant in the gasification stage under N_2. However, it could reach 0.07 %/℃ mass loss in CO_2 atmosphere, which could be attributed to the Boudouard reaction ($C + 2CO_2 \rightarrow 2CO$) [35]. The result

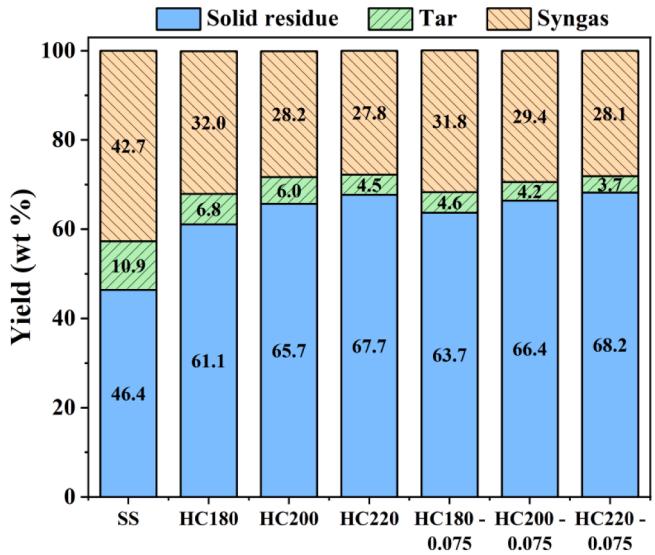

Fig. 4. Products yields in CO_2 gasification of SS and hydrochars at 900 ℃.

indicated that CO_2 atmosphere could achieve significant gasification efficiency and increase the CO fraction.

3.2. Effect of HTC on CO_2 gasification

3.2.1. Comparative gasification of sewage sludge and its hydrochar

The effect of feedstock (SS and HC) on the CO_2 gasification products (SR, tar, syngas) is presented in Fig. 4. The decreased content of organic compounds (C and H content) in HC (Table 2) inhibited the harmful tar production during the CO_2 gasification, which could alleviate the damage of the viscous substances to the reactor in the practical application. The increased SR content could be attributed to the abundant ash content in HC (Table 2). HC with CaO additive could further decrease the tar yield by 17.7–32.4 % at 900 ℃ through catalytic tar cracking reactions [36], therefore increasing the proportion of SR and syngas products. The effect of gasification temperature (700–900 ℃) on the product yields is presented in Fig. S4. The SR yield decreased by 2.7 % and 3.8 % for SS and HC180 respectively when the gasification temperature increased from 700 to 800 ℃, whereas the decrease (7.2 % for SS and 4.4 % for HC180) was enhanced with the further increased temperature (800–900 ℃). This suggested that a higher gasification efficiency can be achieved at a lower gasification temperature when using HC as the gasification feedstock. In addition, the decrease in the tar yield was not obvious anymore for both SS and HC180 when the gasification temperature was increased from 800 to 900 ℃, suggesting that the syngas was mainly produced through Boudouard reaction (Eq. (10)) rather than tar decomposition in this stage.

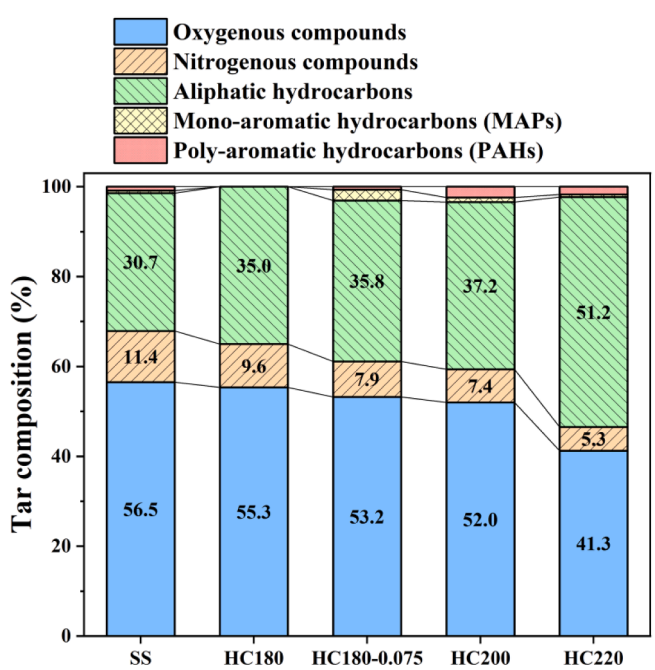

Fig. 5. Chemical composition of tar formed in CO_2 gasification of SS and hydrochars at 900 ℃.

Effect of HTC conditions on the chemical composition of tar from CO_2 gasification is shown in Fig. 5. Tar mainly consisted of five components: 1) oxygenous compounds; 2) nitrogenous compounds; 3) aliphatic hydrocarbons; 4) mono-aromatic hydrocarbons (MAPs); and 5) poly-aromatic hydrocarbons (PAPs) [19,20]. Oxygenous compounds accounted for the largest proportion of the tar composition for SS, then the proportion of oxygenous substances decreased with the elevated HTC temperature. This was related to the lower oxygen content contained in HC produced at higher HTC temperature (Table 2). Besides, gasification of HC derived from higher HTC temperature led to higher percentage of aliphatic hydrocarbons and less nitrogenous and oxygenous compounds in tar (especially for HC220), which is beneficial for tar refining and utilization [37]. Moreover, similar phenomenon was observed when CaO was added in HTC.

The formation and transformation of syngas are summarized in Eqs. (9) to (12) [38,39]. In the initial stage of CO_2 gasification, syngas was produced mainly through thermal cracking of organic matters in feedstock (Eq. (9)). It was found that CO was the primary component (above 60 %) in non-condensable gases (Fig. 6a), which was ascribed to the Boudouard reaction (Eq. (10)). CO could partially react with H_2O and reproduce CO_2 (Eq. (11)). In addition to the Boudouard reaction, the carbon in char could also react with H_2O to form CO and H_2 (Eq. (12)). Under pure CO_2 atmosphere, Boudouard reaction dominated. At 900 ℃, CO yield from gasification of SS was slightly higher than that of HC (Fig. 6a), which was probably associated with reduced carbon in HC and reduced extent of Boudouard reaction [40]. Yields of H_2 and CH_4 from HC were higher than that from SS. However, HC derived from HTC with elevated temperature exhibited slightly higher H_2 yield but lower CH_4 yield. Increased H_2 yield from HC may be related to improved carbonaceous structure, such as improved surface area, pore volume, and enrichment of the alkaline-earth metals (e.g., Ca and K) of HC [41]. Meanwhile, HTC at 180 ℃ with the addition of CaO with Ca/C molar ratio of 0.075 favored H_2 and CO yield. In general, although the yield of CO from SS was slightly higher than that from HC, the total syngas production from HC was higher than that from SS as shown in Fig. 6a. Additionally, the lower heating value (LHV_{gas}) of syngas from HC was higher than that of SS, but the value slightly decreased with the increased HTC temperature and CaO addition (Fig. 6b). These results revealed that HTC pretreatment could not only increase syngas production but also improve the quality of syngas, which could benefit real industrial applications.

Carbon conversion ratio (CCR) is also used to evaluate the gasification efficiency. The CCR of SS and HC180 increased with elevated gasification temperature (Fig. S5). The value dramatically increased when the gasification temperature increased from 800 to 900 ℃, which indicated that Boudouard reaction mainly occurred above 800 ℃ [40]. This is also supported by the significant decreased carbon content of SR when the gasification temperature increased from 800 to 900 ℃ (Table 3).

$$C_xH_yO_z \rightarrow \text{tar} + CO + H_2 + CH_4 + CO_2 + H_2O \quad (9)$$

$$\text{Boudouard reaction: } C + CO_2 \leftrightarrow 2CO \quad (10)$$

$$\text{Water-gas shift reaction: } CO + 2H_2O \leftrightarrow CO_2 + H_2 \quad (11)$$

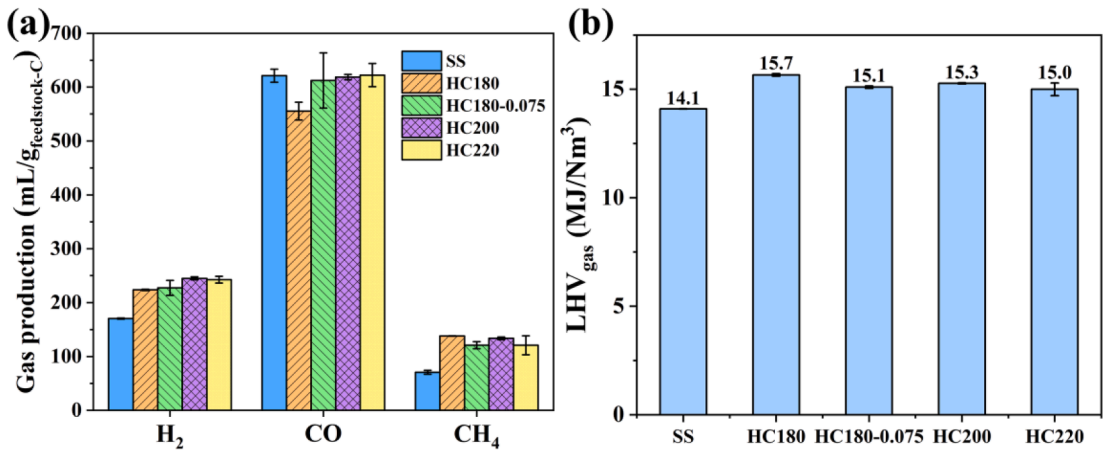

Fig. 6. Effect of hydrothermal condition on (a) syngas production and (b) LHV of syngas during CO_2 gasification at 900 ℃.

Table 3
Elemental composition of solid residues from CO_2 gasification of SS and HCs under different temperatures.

Temperature (℃)	Gasified feedstocks	Ultimate analysis (wt %, db)				Ash (%)
		C	H	N	S	
700	SS	12.87	0.94	1.46	ND	75.26
	HC180	7.49	0.43	0.61	ND	88.40
800	SS	9.32	0.65	1.03	ND	86.69
	HC180	5.43	0.48	0.45	ND	92.78
900	SS	0.79	0.15	0.06	ND	98.55
	HC180	0.59	0.10	0.04	ND	98.99
	HC200	0.57	0.12	0.05	ND	98.85
	HC220	0.63	0.12	0.04	ND	99.00
	HC180-0.075	0.61	0.10	0.05	ND	99.24
	HC200-0.075	0.88	0.12	0.06	ND	98.79
	HC220-0.075	0.56	0.08	0.04	ND	99.16

Solid-water shift reaction: $C + H_2O \leftrightarrow CO + H_2$ (12)

Methanation of CO: $CO + 3H_2 \leftrightarrow CH_4 + H_2O$ (13)

Methanation of CO_2: $CO_2 + 4H_2 \leftrightarrow CH_4 + 2H_2O$ (14)

3.2.2. *Effect of CO_2 concentration*

Effect of CO_2 concentration on the products yield from gasification of SS and HCs is shown in Fig. 7a. With the increased CO_2 concentration, the overall yield of tar and SR decreased while syngas yield increased, with one exception (HC180 as feedstock) that tar yield slightly increased with the increased CO_2 concentration to 20 %. The results suggested that inletting CO_2 could generally reduce harmful tars production which is favor of industrial operations. The presence of CO_2 can enhance thermal cracking of volatiles in biowastes [26] and then reduced tar formation. Therefore, the gasification efficiency could be improved by using CO_2 as gasification agent.

Effect of CO_2 concentration on syngas production is presented in Fig. 8a. Increased CO_2 concentration resulted in an increased CCR (Fig. 7b) and facilitated syngas production, especially CO therein (Fig. 8a), while production of H_2 and CH_4 slightly increased with higher CO_2 concentration. This could result from the enhanced Boudouard reaction, which was further demonstrated by the decreased C and H contents in SRs from gasification with higher CO_2 percentage (Table 4). The increased H_2 yield might be related to the decomposition of organic substance and solid-water–gas shift reactions, and the increased CH_4 was attributed to methanation reactions of CO and CO_2 (Eqs. (13) and (14)) [28,38]. However, increased CO_2 concentration in the gasification process slightly decreased LHV_{gas} (Fig. 8b), which may be attributed to the lower proportion of CH_4 accompanied by higher production of CO. The proportion of CO significantly increased and the concentration of H_2 was relatively lower with the increased CO_2 concentration during the gasification process, resulting in a lower LHV_{gas}. Interestingly, LHV_{gas} of HC180 and HC180-0.075 decreased by 4.2 % and 3.6 %, respectively,

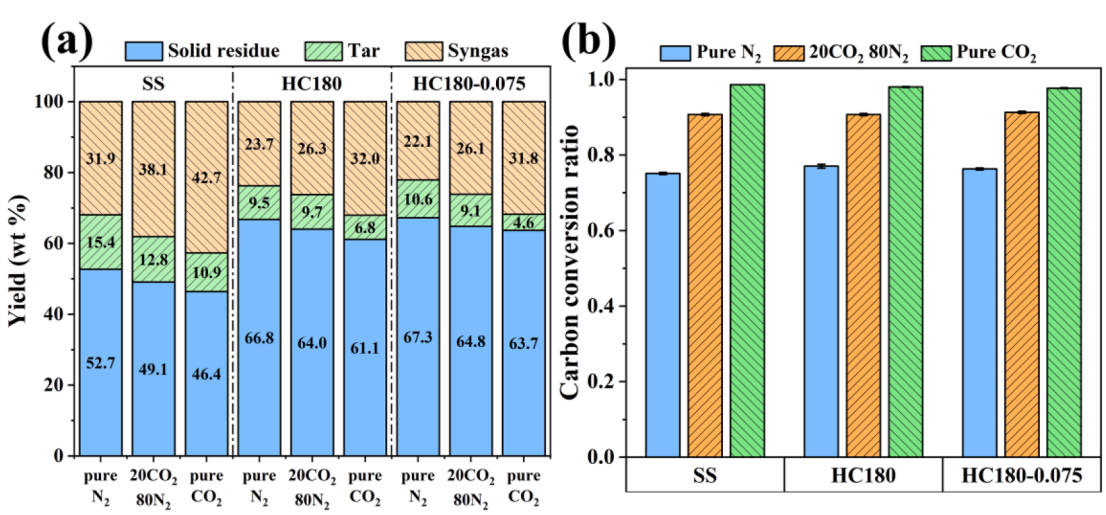

Fig. 7. Effect of CO_2 concentration on (a) yields of three products and (b) carbon conversion ratio during gasification of SS and hydrochars at 900 ℃.

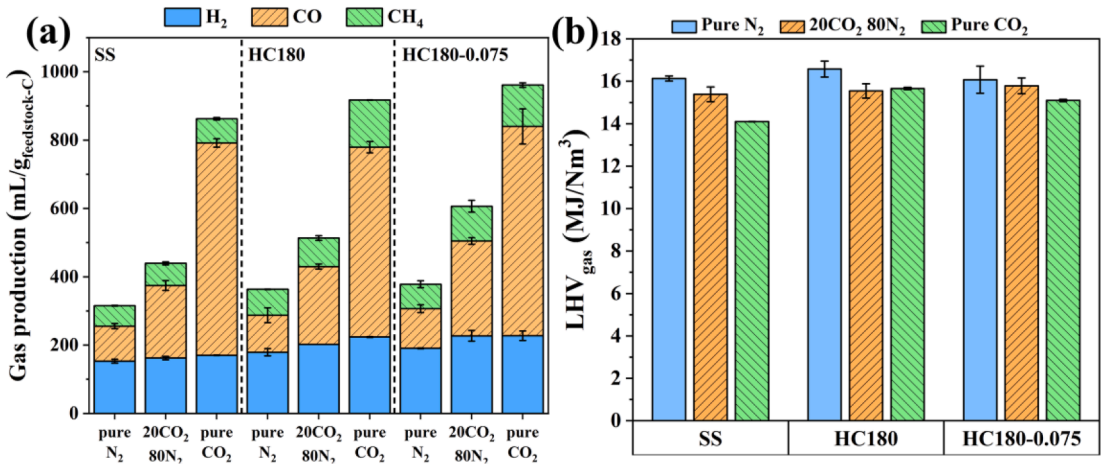

Fig. 8. Effect of CO_2 concentration on (a) typical syngas composition and (b) LHV of syngas during gasification of SS and hydrochars at 900 ℃.

Table 4
Elemental composition of solid residues from gasification of SS and hydrochars at 900 ℃ under different CO_2 concentration.

Samples	Gasification atmosphere	Ultimate analysis (wt.%, db)				Ash (%)
		C	H	N	S	
SS	Pure N_2	12.05	0.45	0.58	ND	75.67
	20CO_2 80 N_2	4.85	0.18	0.21	ND	93.12
	Pure CO_2	0.79	0.15	0.06	ND	98.55
HC180	Pure N_2	6.32	0.30	0.24	ND	92.45
	20CO_2 80 N_2	2.77	0.17	0.11	ND	96.01
	Pure CO_2	0.59	0.10	0.04	ND	99.99
HC180-0.075	Pure N_2	6.01	0.24	0.22	ND	96.03
	20CO_2 80 N_2	2.25	0.22	0.10	ND	97.00
	Pure CO_2	0.61	0.10	0.05	ND	99.24

when the gasification agent was switched from N_2 to CO_2. This drop of LHV_{gas} (12.2 %) was more notable for gasification of SS (Fig. 8b). This suggested that changing gasification agent had less impact on the LHV_{gas} for hydrochars.

3.3. Nitrogen transformation in HTC-CO_2 gasification system

3.3.1. Effect of HTC on nitrogen transformation

In Fig. 9, nitrogen removal efficiency exhibited steady increase from 66.2 % to 76.9 % with increased HTC temperature from 180 to 220 ℃, and this efficiency was further enhanced by 5.3 % for HC180-0.075 with CaO additive. Appropriate amount of CaO could enhance catalytic reaction and thus resulted in dissolution of more reducing sugars and amino acids in the aqueous phase. However, drastic reduction of 4.3 % in nitrogen removal efficiency was found for HC180-0.1 as compared to HC180-0.075. This may imply that formed heterocyclic-N probably deposited onto hydrochars [42] and promoted Maillard reaction. Nevertheless, improvement of nitrogen removal by CaO additive was less significant under higher HTC temperature (200–220 ℃) with only slight increase of 1.7 % and 1.2 % at 200 ℃ and 220 ℃, respectively (Fig. 9a). This could be associated with severe decomposition of *N*-containing substances induced by higher temperature instead of Ca catalysis during HTC. Hence, it is more rationale to carry out hydrothermal pretreatment under lower temperature (ca. 180 ℃) in terms of comparable removal efficiency of nitrogen in HC with less energy consumption.

In HTC, nitrogen was mainly transformed from solid fraction into aqueous phase. Total dissolved nitrogen (TDN) in aqueous phase includes organic-N (Org-N) and inorganic-N (e.g., ammonia-N (NH_4^+-N) and nitrate-N (NO_3^--N)) [14]. In general, TDN concentration presented an upward trend with increasing temperature as a result of enhanced hydrolysis of protein-N and inorganic-N at higher temperature [43], which was in good consistent with remaining N in HC in Table 2. Org-N was predominant in aqueous phase (Fig. 9b). Protein-N was initially decomposed into labile and stable amide-N through the cleavage of peptide bonds which can further form NH_4^+-N via deamination and ring open reactions [14]. However, the addition of CaO resulted in a decreased TDN concentration, which may be due to increased yield of

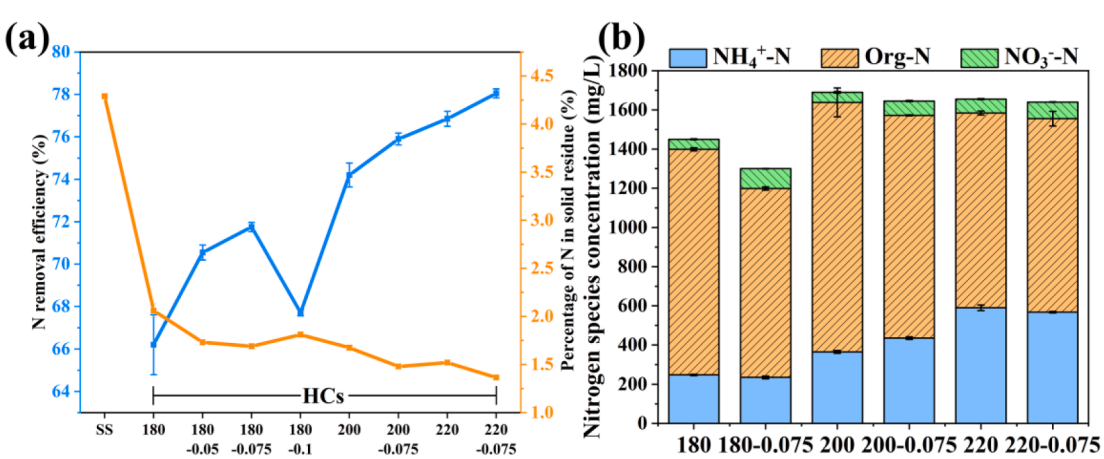

Fig. 9. Effect of temperature and Ca/C molar ratio in HTC on (a) nitrogen removal efficiency and residual nitrogen content in HC, and (b) distribution of nitrogen species in aqueous phase.

aqueous phase. Due to CaO catalysis in HTC, Org-N concentration in aqueous fraction decreased with higher NO_3^--N concentration, thereby contributing to improved N removal efficiency for HC.

Moreover, as N species in HC are crucial in subsequent CO_2 gasification, N 1 s XPS spectra are used to further reveal evolution of different nitrogen functionalities therein (Fig. S6). Specifically, six peaks were observed: (1) pyridine-N (398.8 ± 0.2 eV); (2) protein-N/amine-N/nitrile-N (399.8 ± 0.2 eV); (3) pyrrole-N (400.5 ± 0.2 eV); (4) quaternary-N (401.4 ± 0.2 eV); (5) inorganic-N (402.0 ± 0.5 eV); (6) oxide-N (402–405 eV) [8,44,45]. Relative percentages of N species in SS and HC are depcited in Fig. 10. Nitrogen functionalities in SS mainly consisted of protein-N (80.9 %), inorganic-N (16.1 %) and pyridine-N (3 %). Increased temperature and/or addition of CaO promoted hydrolysis of protein-N and inorganic-N to form NH_4^+-N/NO_3^--N in aqueous phase with complete decomposition of inorganic-N at 220 ℃. At 180 ℃ and 200 ℃, pyrrole-N and quaternary-N were initially formed. Pyridine-N and pyrrole-N can be formed from cyclization of amine, and quaternary-N is originated from polymerization or ring condensation between pyridine-N and pyrrole-N [45,46]. In the presence of CaO, formation of stable quaternary-N started even at 180 ℃, implying the facilitated stabilization of nitrogen in HC induced by CaO. Different from severe decomposition of pyridine-N, pyrrole-N and quaternary-N in near- and super- critical hydrothermal reaction [9], CaO may favor conversion of amine-N into pyrrole-N and the polymerization of pyridine-N into stable quaternary-N, leading to the decreased pyridine-N but increased pyrrole-N and quaternary-N in HC180-0.075 and HC200-0.075 during low temperature HTC in this study. Despite high heterocyclic nitrogen species in HC upon addition of CaO, there were more stable nitrogen functionalities which may require higher activation energy to the bond cleavage, which may be beneficial to reduced emissions of NO_x precursors in CO_2 gasification.

3.3.2. Distribution of nitrogen species during CO_2 gasification

Dynamic transformation of nitrogen is responsible for formation of NO_x precursors in CO_2 gasification. Table 5 demonstrates nitrogen distribution among products from gasification, including char-N, tar-N, NO_x precursors-N and other-N. In CO_2 gasification of SS, both tar-N and char-N gradually decreased while NO_x precursors-N and other-N increased with elevated temperature, which probably resulted from severe decomposition of *N*-containing substances into gases (e.g., NH_3, HCN and N_2) [23]. During CO_2 gasification, less nitrogen was retained in SR, while most of N was transformed into tar or gases, especially at 900 ℃. However, char-N from gasification of HC was higher than that of SS (Table 5), indicating the potential transformation of nitrogen in HC into stable nitrogen species (e.g., quaternary-N) that were retained in SR rather than being released as NO_x precursors-N. This could be confirmed by the increased percentage of quaternary-N in SR derived from HC180 (Fig. 11b). It is speculated that HC could be better gasification feedstock than raw SS from the perspective of promoted stabilization of nitrogen in SR and less emissions of NO_x precursors-N. In addition, lower tar-N was also observed in gasification of HC (Table 5). In particular, there was a remarkable reduction of tar-N (from 28.08 % to 16.02 %) derived from gasification of HC180-0.075 as compared to that of HC180, reflecting the catalytic decomposition of tar as a consequence of metallic components (especially Ca/Fe-based substances) therein [47]. Meanwhile, lower content of NO_x precursors-N but higher content of other-N (e.g., N_2 and other deposits on the inner surface of the quartz tube) may indicate that nitrogen tended to form N_2 during gasification. In this regard, hydrothermal pretreatment with CaO additive (even small amount) could be an efficient strategy to realize mitigated NO_x precursors in CO_2 gasification for SS management.

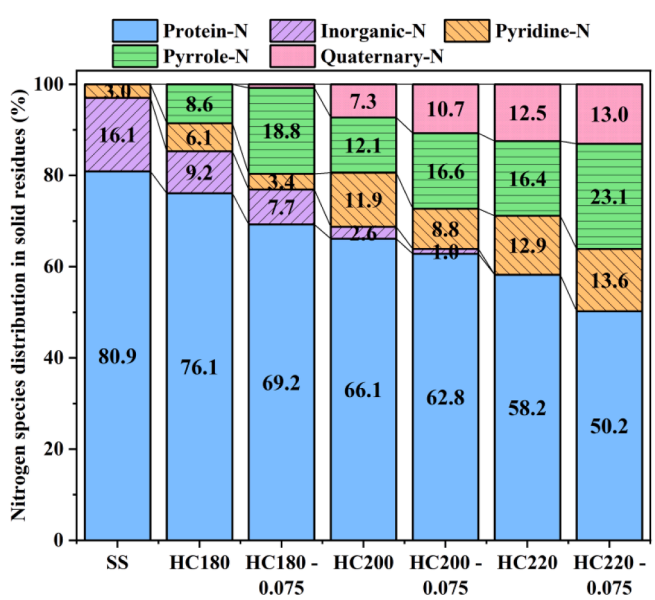

Fig. 10. Evolution of nitrogen species in hydrochars from HTC of SS under various conditions.

3.3.3. Release characteristics of NO_x precursors

Formation of NO_x precursors from CO_2 gasification of SS and HCs can be expressed as yields of NH_3-N and HCN-N. As depicted in Fig. 11, NH_3-N was predominant under all reaction conditions as investigated. Regardless of the feedstock being SS or HCs, yield of NO_x precursors-N (i.e., NH_3-N, HCN-N) generally increased with the increased gasification temperature, suggesting that higher gasification temperature will promote the formation of NH_3-N and HCN-N because of higher activation energies. But yields of NH_3-N and HCN-N from SS were always higher than those from HCs, which was mainly attributed to significantly reduced protein-N and inorganic-N in HC [48,49].

3.3.3.1. Fate of HCN in NO_x precursors. Pyrrole-N in both char-N and tar-N was the main source of HCN. Although there was an increase of pyrrole-N in HCs after HTC (Fig. 10), formation of HCN eventually decreased because HTC also reduced the tar yield (Fig. 7a). Overall, higher gasification temperature led to higher quaternary-N but lower pyridine-N and pyrrole-N in SRs, which was obvious at 900 °C (Fig. 11b). It is assumed that the pyrrole-N and pyridine-N in SR could be polymerized into quaternary-N or decomposed to form NH_3 and HCN through dehydrogenation or ring scission [50], resulting in increased emissions of NO_x precursors. When temperature was elevated from 700 to 800 ℃ in CO_2 gasification of SS, HCN yield was increased by 47.0 % (Fig. 11a), while the content of pyrrole-N dramatically decreased by 11.9 % (Fig. 11b). But the content of pyrrole-N was only reduced by 2.6 % and there was no obvious change for HCN emissions when the temperature was further increased to 900 ℃. Thus, it could be deduced that the decomposition of pyrrole-N in char mainly promoted the HCN emission from SS around 800 ℃. As for gasification of HC180, the most significant reduction of pyrrole-N and HCN formation was observed when the gasification temperature was increased from 800 to 900 ℃ (Fig. 11a and b). It is probably related to more stable nitrogen in HC and higher gasification temperature was required to promote the transformation of pyrrole-N and pyridine-N in HC to quaternary-N. This could be evidenced by the exceptionally high content of quaternary-N (45.9 %) in SR from gasification of HC180 at 900 ℃.

3.3.3.2. Fate of NH_3 in NO_x precursors. With the elevated temperature, emission of NH_3-N from CO_2 gasification of SS and HC increased steadily (Fig. 11a) and remaining nitrogen in SRs decreased (Table 3). The decreasing content of pyrrole-N and pyridine-N in SRs (Fig. 11b) could be responsible for enhanced formation of NH_3-N/HCN with the increased gasification temperature. Moreover, higher quaternary-N content in SRs (Fig. 11b) but much lower yield of NO_x precursors

Table 5
Distribution of nitrogen in products from CO_2 gasification.

Sample	Temperature (℃)	N in feedstock (%)	N in hydrochars (%)	N in gasification products (%)			
				Char-N	Tar-N	NO_x precursors-N	Other-N
SS	700	100 (4.29)	–	19.16	49.69	0.42	30.73
SS	800	100 (4.29)	–	12.87	37.84	0.47	48.81
SS		100 (4.29)	–	0.65	28.99	0.58	69.78
HC180		–	100 (2.06)	1.22	28.08	0.29	70.42
HC180-0.075	900	–	100 (1.69)	1.41	16.02	0.22	82.35
HC200		–	100 (1.67)	1.97	26.53	0.17	71.33
HC220		–	100 (1.52)	1.79	12.31	0.14	85.76

Note: The values in the bracket of N in feedstock or hydrochars are the results from ultimate analysis.

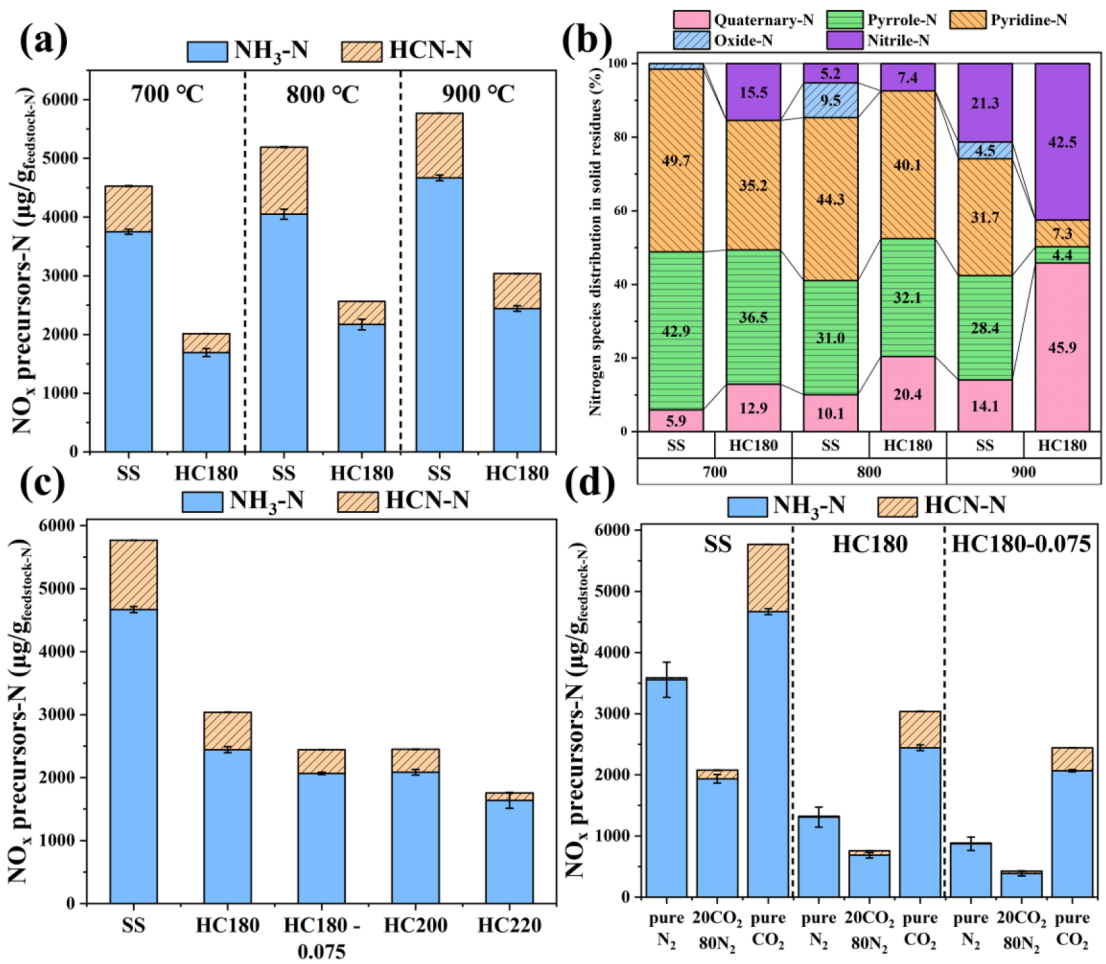

Fig. 11. Effect of gasification temperature on (a) production of NH_3-N and HCN-N and (b) distribution of nitrogen species in biochar from gasification in pure CO_2 atmosphere; (c) Effect of HTC condition on production of NH_3-N and HCN-N in pure CO_2 gasification at 900 ℃, and (d) Effect of CO_2 concentration on production of NH_3-N and HCN-N in gasification at 900 ℃.

Table 6
Main nitrogen-containing compounds in tar after CO_2 gasification.

Gasified feedstocks	Temperature (℃)	Relative content (%)						
		Total *N*-containing compounds	Amines and amides	Nitriles	Heterocyclic-N compounds			
					Pyridine	Indole	Quinoline	Other
SS	700	16.99	5.76	3.38	0.85	4.54	0.72	1.74
SS	800	14.39	5.08	1.39	1.39	5.78	1.50	0.69
SS	900	11.40	3.64	0.26	1.02	7.61	1.12	1.44
HC180		10.83	3.45	1.64	–	4.98	–	0.76
HC180-0.075		7.91	1.10	0.68	–	3.12	2.00	1.01
HC200		7.37	0.75	1.29	1.40	2.27	0.77	0.88
HC220		5.26	0.43	1.31	0.53	2.03	0.60	0.36

(Fig. 11c) from gasification of HCs were found, revealing that the polymerization and/or ring condensation of pyrrole-N and pyridine-N prevailed over their decomposition into NH_3 or HCN [51].

3.3.3.3. Effect of HTC and CO_2 concentration on NO_x precursors. As shown in Fig. 11c, increased HTC temperature favored the reduced yield of NO_x precursors from CO_2 gasification at 900 ℃, especially the reduction of HCN to a negligible amount for HC220, which was closely linked to lower nitrogen content therein (Table 2). Apart from that, HC derived from higher HTC temperature contained more ash and less VM, which could facilitate the reduction of tar formation. Moreover, as aforementioned, nitrogen transformation into stable nitrogen in SRs prevailed in gasification of HC. Higher HTC temperature (>200 ℃) led to a dramatic reduction of amines and amides in tar (Table 6), thereby having a positive effect on reducing the yield of HCN. Furthermore, in Fig. 11c, even a low amount of CaO could further decrease the release of NO_x precursors (especially HCN) from gasification of HC180-0.075, which was even lower than that from HC200. It can be concluded that addition of CaO at lower HTC temperature could efficiently inhibit the release of NO_x precursors from gasification.

Regardless of the gasification atmosphere, HTC pretreatment, especially with CaO additive, could greatly hinder the emissions of NO_x precursors. On the other hand, CO_2 concentration in the gasification process had a significant effect on emissions of NH_3 and HCN (Fig. 11d). Interestingly, HCN emission was negligible under N_2 gasification but the highest release of NO_x precursors (particularly HCN) was noticed in CO_2 gasification of SS and HCs. Nevertheless, introducing 20 % CO_2 could remarkably inhibit the release of NH_3 and HCN. It is assumed that small amount of CO_2 could beneficially consume carbon and catalyze the transformation from NH_3/HCN to N_2 [23]. As compared to N_2 gasification, there was a slight increase of HCN in gasification under 20 % CO_2 + 80 % N_2. This further confirmed that the existence of CO_2 and N_2 enhanced the thermal cracking of *N*-containing in chars which was regarded as the primary source of HCN-N release [26]. However, pure CO_2 atmosphere was detrimental to the reduction of NO_x precursors. Excessive CO_2 might offer sufficient catalytic thermal cracking of *N*-containing compounds in tar/char to form more NH_3 and HCN. Meanwhile, the Boudouard reaction between char and CO_2 could consume a large amount of carbon in chars, causing more active sites for promoted decomposition of nitrogen functionalities and CO_2. Gasification of HC180-0.075 under 20 %CO_2 + 80 % N_2 demonstrated the lowest release of NO_x precursors-N (less than 500 μg/$g_{feedstock\text{-}N}$). To conclude, the HTC-CO_2 gasification system can achieve considerately mitigated emissions of NH_3 and HCN through low temperature hydrothermal pretreatment of SS with CaO and injecting gasification agent containing a lower CO_2 concentration (ca. 20 %).

3.4. Mechanism for reduction of NO_x precursors in HTC-CO_2 gasification system

Investigation of nitrogen conversion pathways is essential to elaborate the mechanism for reduction of NO_x precursors in this proposed system. Based on aforementioned data analysis, the plausible nitrogen conversion pathways into NO_x precursors can be clearly described in Fig. 12. Nitrogen species originating from protein-N in SS were the main contributor to *N*-containing compounds. During HTC process, partial protein-N was decomposed into amine-N that could be transformed into NH_3 or HCN in CO_2 gasification [42]. Inorganic-N can be also decomposed into NH_3 through thermal decomposition of ammonium-containing substances. In addition, protein-N could be converted into pyrrole-N or pyridine-N by cyclization or dimerization, and these nitrogen species could be subsequently transformed into quaternary-N [46]. During these reactions, pyridine-N and pyrrole-N could partially generate NH_3 and HCN through hydrogenation with H radical and ring-opening, respectively [52,53]. Besides, the amine-N derived from protein-N, which existed in char or tar, could react with H radical to form HCNO which could be easily decomposed into HCN [54].

Obvious decrease in NH_3-N emissions from gasification of HC mainly resulted from the lower content of inorganic-N and protein-N, which weakened the decomposition of inorganic-N and depolymerization of labile protein-N. Inorganic-N was completely removed from HC after HTC. Meanwhile, protein-N (especially labile proteins) in SS was also hydrolyzed, leading to a decrease in NH_3-N by 47.7 to 64.9 % from gasification of HC180 and HC220, respectively. The addition of CaO could greatly reduce the proportion of protein-N and inorganic-N, which may achieve a lower emission level of NH_3. In addition, increased ash

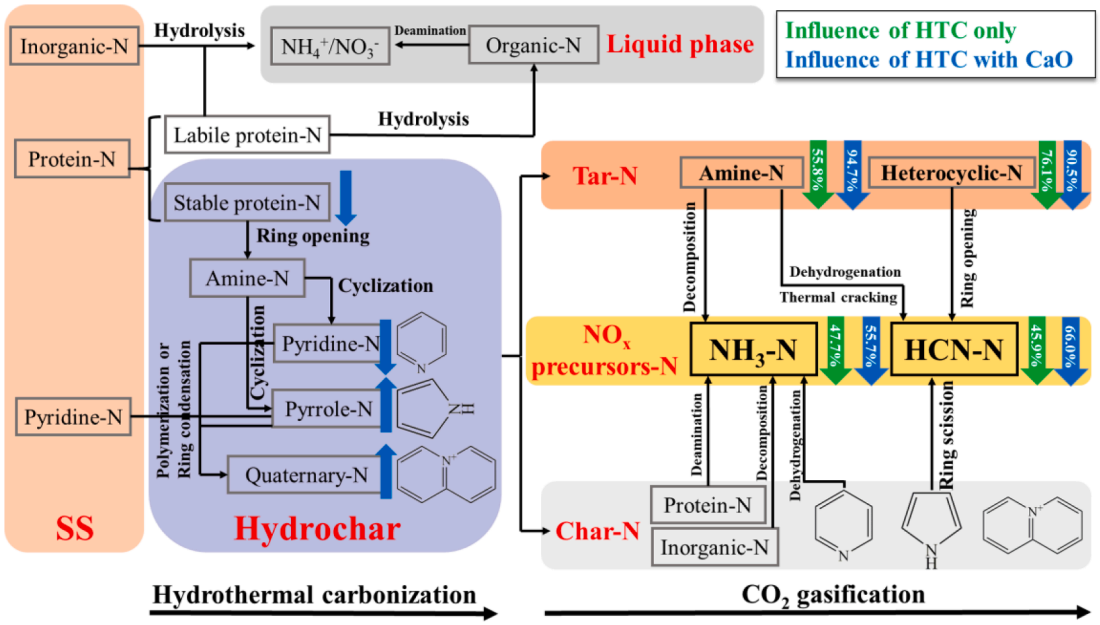

Fig. 12. Schematic illustration of nitrogen transformation pathways in the entire HTC-CO_2 gasification system (Blue arrows indicate the influence of CaO additive in HTC on nitrogen species in hydrochar and its gasification products, while green arrows indicate the influence of HTC (Temperature: 180 ℃ and Ca/C molar ratio of 0.075) on the formation of tar-N and NO_x precursors-N as compared to direct SS gasification).

content (especially minerals) in HC was assumed to benefit the reduced yield of NH_3 via mineral-based catalytic thermal cracking of chars [55]. On the one hand, after HTC with CaO, stable protein-N tended to be converted into heterocyclic-N that can be involved in dehydrogenation to generate NH_3 during gasification. At the same time, quaternary-N, a more stable form of heterocyclic-N, was also formed, which can hinder NH_3 formation [8]. Higher HTC temperature and CaO additive would accelerate the formation of quaternary-N to prevent emissions of NO_x precursors. The decrease of active *N*-containing compounds (i.e., protein-N, inorganic-N) and the increase of stable quaternary-N in HC could be responsible for selective N conversion into char-N instead of gas phase, thus reducing the yield of NO_x precursors. On the other hand, Tian et al. [48] reported that the ring-opening of heterocyclic-N in tars could contribute to the release of NH_3-N accounting for about 18.3 % of N in SS. In this study, HTC pretreatment largely reduced tar formation (Fig. 4), leading to a decrease in NH_3 emission. With the increased gasification and HTC temperature, amines and amides in tar showed a downward trend (Table 6), which was beneficial to reduce NH_3 yield. As a result, a significant decrease of NH_3 occurred owing to 1) HC derived from HTC containing little labile protein-N and more non-active quaternary-N; and 2) less tar yield and tar-N content as compared to CO_2 gasification of raw SS.

As elaborated in Fig. 12, in gasification stage, the emission of HCN-N was mainly linked to the secondary reactions of primary intermediates, including amine-N and heterocyclic-N in tars, and/or pyrrole-N in chars [49]. In HTC stage, some protein-N could be hydrolyzed and deaminated into NH_4^+-N in aqueous phase, resulting in decreasing amine-N in char and thus reduced breakdown of amine-N in tars. In gasification of HCs (especially with CaO), tar yield together with the content of amine-N and heterocyclic-N compounds in tars were decreased (Table 6). These changes significantly contributed to the great reduction of HCN yield.

In addition, the presence of inorganic minerals (such as Fe and Ca species) in ash could facilitate the transformation of NH_3 and HCN into N_2 [56]. Injecting CaO or other Ca-containing materials could further promote transformation of NH_3 or HCN to to N_2 or syngas in gasification above 500 ℃ via Eqs. (15)-(18) [57]. Hence, the increased ash, particularly Fe and Ca, in HC after HTC with CaO, would have a positive catalytic effect on inhibited release of NO_x precursors.

$$CaO/Ca^{2+} + \text{heterocyclic-N} \rightarrow N_2 + CaC_xH_y \tag{15}$$

$$CaO/Ca^{2+} + \text{Pyrrole-N/Pyridine-N} \rightarrow H_2/CO + CaC_xN_y \tag{16}$$

$$CaC_xN_y \rightarrow N_2 + CaC_x \tag{17}$$

$$CaO/Ca^{2+} + HCN/NH_3 \rightarrow CaC_xN_y + H_2/CO \tag{18}$$

To sum up, emissions of NO_x precursors in SS management can be successfully controlled in HTC-CO_2 gasification system. During HTC pretreatment with Ca-based additives, labile protein-N was primarily removed and stable protein-N was substantially stabilized, remarkably contributing to promoted N conversion from heterocyclic-N and/or NH_3/HCN to N_2. In CO_2 gasification, manipulation and optimization of CO_2 percentage in the gasification agent will considerably prevent emissions of NH_3 and HCN.

4. Conclusion

The sequential low temperature hydrothermal pretreatment and CO_2 gasification system has been applied for SS treatment to remarkably improve the yield and quality of formed syngas. In particular, HTC pretreatment and CaO additive could facilitate the transformation of pyridine-N into pyrrole-N and quaternary-N in HC, thereby improving the stability of nitrogen therein. Furthermore, CO_2 gasification of HC demonstrated distinct advantages over direct gasification of raw SS from perspectives of decreased formation of tar with less oxygenous and nitrogenous compounds, and enhanced syngas yield, from 861 mL/$g_{feedstock\text{-}C}$ for SS to 959 mL/$g_{feedstock\text{-}C}$ for HC, with distinctly mitigated formation of NH_3-N and HCN-N high up to 69.6 %. The HTC pretreatment with CaO greatly contributed to the reduced release of NH_3 and HCN due to reduced nitrogen (from 4.29 % in SS to 1.36 % in HC) and stable quaternary-N in HC, and calcium catalyzed cracking of nitrogenous tar. In addition, CO_2 gasification improved the carbon conversion efficiency and tar decomposition via Boudouard reaction, leading to obvious increase of syngas yield. However, higher CO_2 atmosphere (e.g., 100 %) in gasification was detrimental to the decrease of NO_x precursors. This could be associated with CO_2 promoted thermal cracking of *N*-containing compounds in tar/char to produce more NH_3 and HCN than those transformed into N_2. Surprisingly, 20 % CO_2 greatly inhibited the formation of NO_x precursors from gasification. Overall, this HTC-CO_2 gasification process reveals promising strategies for sustainable SS management towards enhanced high-quality syngas production.

CRediT authorship contribution statement

Weiming Huang: Investigation, Data curation, Writing – original draft. **Ruichi Zhang:** Investigation, Writing – review & editing. **Apostolos Giannis:** Writing – review & editing. **Chuanhao Li:** Resources. **Chao He:** Conceptualization, Writing – review & editing, Project administration, Funding acquisition.

Declaration of Competing Interest

The authors declare that they have no known competing financial interests or personal relationships that could have appeared to influence the work reported in this paper.

Data availability

Data will be made available on request.

Acknowledgements

This research work is financially supported by the National Natural Science Foundation of China (No. 51906264). C.H. acknowledges the Academy Research Fellowship and its research project funded by Academy of Finland (decision numbers: 341052, 346578). C.L. thanks Science and Technology Planning Project of Guangdong Province (2020A0505100032).

Appendix A. Supplementary data

Supplementary data to this article can be found online at https://doi.org/10.1016/j.cej.2022.140239.

References

[1] B. Wu, S.M. Berg, C.K. Remucal, T.J. Strathmann, Evolution of N-Containing Compounds during Hydrothermal Liquefaction of Sewage Sludge, ACS Sustainable Chem. Eng. 8 (49) (2020) 18303–18313, https://doi.org/10.1021/acssuschemeng.0c07060.

[2] Y.D. Chen, R. Wang, X. Duan, S. Wang, N.Q. Ren, S.H. Ho, Production, properties, and catalytic applications of sludge derived biochar for environmental remediation, Water Res 187 (2020), 116390, https://doi.org/10.1016/j.watres.2020.116390.

[3] G. Chen, X. Wang, J. Li, B. Yan, Y. Wang, X. Wu, R. Velichkova, Z. Cheng, W. Ma, Environmental, energy, and economic analysis of integrated treatment of municipal solid waste and sewage sludge: A case study in China, Sci Total Environ 647 (2019) 1433–1443, https://doi.org/10.1016/j.scitotenv.2018.08.104.

[4] N. Gao, K. Kamran, C. Quan, P.T. Williams, Thermochemical conversion of sewage sludge: A critical review, Prog. Energy Combust. Sci. 79 (2020), https://doi.org/10.1016/j.pecs.2020.100843.

[5] G. Lopez, M. Artetxe, M. Amutio, J. Alvarez, J. Bilbao, M. Olazar, Recent advances in the gasification of waste plastics. A critical overview, Renew. Sustain. Energy Rev. 82 (2018) 576–596, https://doi.org/10.1016/j.rser.2017.09.032.

[6] A. Ramos, E. Monteiro, V. Silva, A. Rouboa, Co-gasification and recent developments on waste-to-energy conversion: A review, Renew. Sustain. Energy Rev. 81 (2018) 380–398, https://doi.org/10.1016/j.rser.2017.07.025.

[7] W.-J. Liu, Z.-G. Shao, Y. Xu, Emission characteristics of nitrogen and sulfur containing pollutants during the pyrolysis of oily sludge with and without catalysis, J. Hazard. Mater. 401 (2021), 123820, https://doi.org/10.1016/j.jhazmat.2020.123820.

[8] X. Zhuang, Y. Song, X. Wang, H. Zhan, X. Yin, C. Wu, P. Wang, Pyrolysis of hydrothermally pretreated biowastes: The controllability on the formation of NO precursors, Chem. Eng. J. 393 (2020), 124727, https://doi.org/10.1016/j.cej.2020.124727.

[9] C. He, K. Wang, Y. Yang, P.N. Amaniampong, J.Y. Wang, Effective nitrogen removal and recovery from dewatered sewage sludge using a novel integrated system of accelerated hydrothermal deamination and air stripping, Environ Sci Technol 49 (11) (2015) 6872–6880, https://doi.org/10.1021/acs.est.5b00652.

[10] G. Chen, J. Li, K. Li, F. Lin, W. Tian, L. Che, B. Yan, W. Ma, Y. Song, Nitrogen, sulfur, chlorine containing pollutants releasing characteristics during pyrolysis and combustion of oily sludge, Fuel 273 (2020), 117772, https://doi.org/10.1016/j.fuel.2020.117772.

[11] H. Zhan, X. Zhuang, Y. Song, G. Chang, Z. Wang, X. Yin, X. Wang, C. Wu, Formation and regulatory mechanisms of N-containing gaseous pollutants during stage-pyrolysis of agricultural biowastes, J. Cleaner Prod. 236 (2019), 117706, https://doi.org/10.1016/j.jclepro.2019.117706.

[12] Q. Ren, C. Zhao, NO_x and N_2O precursors from biomass pyrolysis: role of cellulose, hemicellulose and lignin, Environ Sci Technol 47 (15) (2013) 8955–8961, https://doi.org/10.1021/es4017574.

[13] T. Wang, Y. Zhai, Y. Zhu, C. Li, G. Zeng, A review of the hydrothermal carbonization of biomass waste for hydrochar formation: Process conditions, fundamentals, and physicochemical properties, Renew. Sustain. Energy Rev. 90 (2018) 223–247, https://doi.org/10.1016/j.rser.2018.03.071.

[14] X. Zhuang, Y. Huang, Y. Song, H. Zhan, X. Yin, C. Wu, The transformation pathways of nitrogen in sewage sludge during hydrothermal treatment, Bioresour. Technol. 245 (2017) 463–470, https://doi.org/10.1016/j.biortech.2017.08.195.

[15] D. Kim, K. Lee, K.Y. Park, Hydrothermal carbonization of anaerobically digested sludge for solid fuel production and energy recovery, Fuel 130 (2014) 120–125, https://doi.org/10.1016/j.fuel.2014.04.030.

[16] Y. Feng, T. Yu, D. Chen, G. Xu, L. Wan, Q. Zhang, Y. Hu, Effect of Hydrothermal Treatment on the Steam Gasification Behavior of Sewage Sludge: Reactivity and Nitrogen Emission, Energy Fuels 32 (1) (2018) 581–587, https://doi.org/10.1021/acs.energyfuels.7b03304.

[17] Y. Shen, C. He, X. Chen, A.A. Lapkin, W. Xiao, C.-H. Wang, Nitrogen Removal and Energy Recovery from Sewage Sludge by Combined Hydrothermal Pretreatment and CO_2 Gasification, ACS Sustainable Chem. Eng. 6 (12) (2018) 16629–16636, https://doi.org/10.1021/acssuschemeng.8b03857.

[18] P. Zhao, H. Chen, S. Ge, K. Yoshikawa, Effect of the hydrothermal pretreatment for the reduction of NO emission from sewage sludge combustion, Appl. Energy 111 (2013) 199–205, https://doi.org/10.1016/j.apenergy.2013.05.029.

[19] Y. Feng, T. Yu, K. Ma, G. Xu, Y. Hu, D. Chen, Effect of Hydrothermal Temperature on the Steam Gasification Performance of Sewage Sludge: Syngas Quality and Tar Formation, Energy Fuels 32 (6) (2018) 6834–6838, https://doi.org/10.1021/acs.energyfuels.8b00696.

[20] X. Zhuang, Y. Song, H. Zhan, X. Yin, C. Wu, Gasification performance of biowaste-derived hydrochar: The properties of products and the conversion processes, Fuel 260 (2020), 116320, https://doi.org/10.1016/j.fuel.2019.116320.

[21] J. Moon, T.-Y. Mun, W. Yang, U. Lee, J. Hwang, E. Jang, C. Choi, Effects of hydrothermal treatment of sewage sludge on pyrolysis and steam gasification, Energy Convers. Manage. 103 (2015) 401–407, https://doi.org/10.1016/j.enconman.2015.06.058.

[22] S. Chen, Z. Zhao, A. Soomro, S. Ma, M. Wu, Z. Sun, W. Xiang, Hydrogen-rich syngas production via sorption-enhanced steam gasification of sewage sludge, Biomass Bioenergy 138 (2020), 105607, https://doi.org/10.1016/j.biombioe.2020.105607.

[23] Q. Zhang, H. Liu, G. Lu, L. Yi, H. Hu, H. Chi, H. Yao, Mechanism of conditioner CaO on NO_x precursors evolution during sludge steam gasification, Proc. Combust. Inst. 36 (3) (2017) 4003–4010, https://doi.org/10.1016/j.proci.2016.09.006.

[24] L. Peng, Y. Wang, Z. Lei, G. Cheng, Co-gasification of wet sewage sludge and forestry waste in situ steam agent, Bioresour. Technol. 114 (2012) 698–702, https://doi.org/10.1016/j.biortech.2012.03.079.

[25] A.A. Ahmad, N.A. Zawawi, F.H. Kasim, A. Inayat, A. Khasri, Assessing the gasification performance of biomass: A review on biomass gasification process conditions, optimization and economic evaluation, Renew. Sustain. Energy Rev. 53 (2016) 1333–1347, https://doi.org/10.1016/j.rser.2015.09.030.

[26] J. Lee, X. Yang, S.-H. Cho, J.-K. Kim, S.S. Lee, D.C.W. Tsang, Y.S. Ok, E.E. Kwon, Pyrolysis process of agricultural waste using CO_2 for waste management, energy recovery, and biochar fabrication, Appl. Energy 185 (2017) 214–222, https://doi.org/10.1016/j.apenergy.2016.10.092.

[27] M. Jeremiáš, M. Pohořelý, K. Svoboda, S. Skoblia, Z. Beňo, M. Šyc, CO_2 gasification of biomass: The effect of lime concentration in a fluidised bed, Appl. Energy 217 (2018) 361–368, https://doi.org/10.1016/j.apenergy.2018.02.151.

[28] B. Prabowo, K. Umeki, M. Yan, M.R. Nakamura, M.J. Castaldi, K. Yoshikawa, CO_2–steam mixture for direct and indirect gasification of rice straw in a downdraft gasifier: Laboratory-scale experiments and performance prediction, Appl. Energy 113 (2014) 670–679, https://doi.org/10.1016/j.apenergy.2013.08.022.

[29] G. Chen, R. Yang, Z. Cheng, B. Yan, W. Ma, Nitric oxide formation during corn straw/sewage sludge co-pyrolysis/gasification, J. Cleaner Prod. 197 (2018) 97–105, https://doi.org/10.1016/j.jclepro.2018.06.073.

[30] Z.-X. Xu, Y.-Q. Shan, Z. Zhang, X.-Q. Deng, Y. Yang, R. Luque, P.-G. Duan, Hydrothermal carbonization of sewage sludge: effect of inorganic salts on hydrochar's physicochemical properties, Green Chem. 22 (2020) 7010–7022, https://doi.org/10.1039/d0gc02615h.

[31] B. Biswas, A. Kumar, A.C. Fernandes, K. Saini, S. Negi, U.D. Muraleedharan, T. Bhaskar, Solid base catalytic hydrothermal liquefaction of macroalgae: Effects of process parameter on product yield and characterization, Bioresour Technol 307 (2020), 123232, https://doi.org/10.1016/j.biortech.2020.123232.

[32] Y.-Q. Shan, X.-Q. Deng, R. Luque, Z.-X. Xu, L. Yan, P.-G. Duan, Hydrothermal carbonization of activated sewage sludge over ammonia-treated Fenton sludge to produce hydrochar for clean fuel use, Green Chem. 22 (15) (2020) 5077–5083, https://doi.org/10.1039/d0gc01701a.

[33] C. He, A. Giannis, J.-Y. Wang, Conversion of sewage sludge to clean solid fuel using hydrothermal carbonization: Hydrochar fuel characteristics and combustion behavior, Appl. Energy 111 (2013) 257–266, https://doi.org/10.1016/j.apenergy.2013.04.084.

[34] X. Lu, X. Ma, X. Chen, Co-hydrothermal carbonization of sewage sludge and lignocellulosic biomass: Fuel properties and heavy metal transformation behaviour of hydrochars, Energy 221 (2021), 119896, https://doi.org/10.1016/j.energy.2021.119896.

[35] T. Dahou, F. Defoort, B. Khiari, M. Labaki, C. Dupont, M. Jeguirim, Role of inorganics on the biomass char gasification reactivity: A review involving reaction mechanisms and kinetics models, Renew. Sustain. Energy Rev. 135 (2021), 110136, https://doi.org/10.1016/j.rser.2020.110136.

[36] G. Tang, J. Gu, G. Wei, H. Yuan, Y. Chen, Reaction Performance and Mechanism of a $NiO/Ca_2Fe_2O_5$ Oxygen Carrier in Chemical Looping Gasification of Cellulose, Chem. Eng. J. (2022), 137516, https://doi.org/10.1016/j.cej.2022.137516.

[37] L. Zhang, R. Liu, R. Yin, Y. Mei, Upgrading of bio-oil from biomass fast pyrolysis in China: A review, Renew. Sustain. Energy Rev. 24 (2013) 66–72, https://doi.org/10.1016/j.rser.2013.03.027.

[38] C. He, C.-L. Chen, A. Giannis, Y. Yang, J.-Y. Wang, Hydrothermal gasification of sewage sludge and model compounds for renewable hydrogen production: A review, Renew. Sustain. Energy Rev. 39 (2014) 1127–1142, https://doi.org/10.1016/j.rser.2014.07.141.

[39] H. Sun, C. Wu, Autothermal CaO Looping Biomass Gasification for Renewable Syngas Production, Environ Sci Technol 53 (15) (2019) 9298–9305, https://doi.org/10.1021/acs.est.9b01527.

[40] F. Girard-Sahun, O. Biondo, G. Trenchev, G. van Rooij, A. Bogaerts, Carbon bed post-plasma to enhance the CO_2 conversion and remove O_2 from the product stream, Chem. Eng. J. 442 (2022), 136268, https://doi.org/10.1016/j.cej.2022.136268.

[41] Z. Zhang, Z. Zhu, B. Shen, L. Liu, Insights into biochar and hydrochar production and applications: A review, Energy 171 (2019) 581–598, https://doi.org/10.1016/j.energy.2019.01.035.

[42] L. Leng, L. Yang, S. Leng, W. Zhang, Y. Zhou, H. Peng, H. Li, Y. Hu, S. Jiang, H. Li, A review on nitrogen transformation in hydrochar during hydrothermal carbonization of biomass containing nitrogen, Sci Total Environ 756 (2021), 143679, https://doi.org/10.1016/j.scitotenv.2020.143679.

[43] W. Huang, T. Yuan, Z. Zhao, X. Yang, W. Huang, Z. Zhang, Z. Lei, Coupling Hydrothermal Treatment with Stripping Technology for Fast Ammonia Release and Effective Nitrogen Recovery from Chicken Manure, ACS Sustainable Chem. Eng. 4 (7) (2016) 3704–3711, https://doi.org/10.1021/acssuschemeng.6b00315.

[44] N. Wang, H. Zhan, X. Zhuang, B. Xu, X. Yin, X. Wang, C. Wu, Torrefaction of waste wood-based panels: More understanding from the combination of upgrading and denitrogenation properties, Fuel Process. Technol. 206 (2020), 106462, https://doi.org/10.1016/j.fuproc.2020.106462.

[45] R. Wang, H. Lei, S. Liu, X. Ye, J. Jia, Z. Zhao, The redistribution and migration mechanism of nitrogen in the hydrothermal cocarbonization process of sewage sludge and lignocellulosic wastes, Sci Total Environ 776 (2021), 145922, https://doi.org/10.1016/j.scitotenv.2021.145922.

[46] J. Huang, Z. Wang, Y. Qiao, B. Wang, Y. Yu, M. Xu, Transformation of nitrogen during hydrothermal carbonization of sewage sludge: Effects of temperature and Na/Ca acetates addition, Proc. Combust. Inst. 38 (3) (2020) 4335–4344, https://doi.org/10.1016/j.proci.2020.06.075.

[47] Y. Wang, M. Liu, N. Dong, Y. Lin, G. Chang, G. Wei, K. Zhao, X. Wang, A. Zheng, Z. Zhao, Z. Huang, Y. Fang, H. Li, Chemical looping gasification of high nitrogen wood waste using a copper slag oxygen carrier modified by alkali and alkaline earth metals, Chem. Eng. J. 410 (2021), 128344, https://doi.org/10.1016/j.cej.2020.128344.

[48] Y. Tian, J. Zhang, W. Zuo, L. Chen, Y. Cui, T. Tan, Nitrogen conversion in relation to NH_3 and HCN during microwave pyrolysis of sewage sludge, Environ Sci Technol 47 (7) (2013) 3498–3505, https://doi.org/10.1021/es304248j.

[49] H. Zhan, X. Zhuang, Y. Song, X. Yin, C. Wu, Insights into the evolution of fuel-N to NO_x precursors during pyrolysis of N-rich nonlignocellulosic biomass, Appl. Energy 219 (2018) 20–33, https://doi.org/10.1016/j.apenergy.2018.03.015.

[50] K. Tian, W.J. Liu, T.T. Qian, H. Jiang, H.Q. Yu, Investigation on the evolution of N-containing organic compounds during pyrolysis of sewage sludge, Environ Sci Technol 48 (18) (2014) 10888–10896, https://doi.org/10.1021/es5022137.

[51] H. Jiang, X. Chen, S. Chen, H. Li, Y. Peng, A. Zhu, C. Charles Xu, W. Yang, Recovery of arsenic and practical utilization of aqueous phase in hydrothermal liquefaction of hyperaccumulator, Chem. Eng. J. 439 (2022), 135514, https://doi.org/10.1016/j.cej.2022.135514.

[52] Z. Wang, Z. Wang, Z. Sun, K. Ma, L. Du, R. Yuan, Evolution of S/N containing compounds in pyrolysis of highly oily petroleum sludge, Fuel 318 (2022), 123687, https://doi.org/10.1016/j.fuel.2022.123687.

[53] X. Niu, L. Shen, Evolution of carbon and nitrogen during chemical looping gasification of rapeseed cake with Ca-Fe oxygen carrier, Chem. Eng. J. 431 (2022), 134232, https://doi.org/10.1016/j.cej.2021.134232.

[54] D. Xu, L. Yang, M. Zhao, J. Zhang, S.S.A. Syed-Hassan, H. Sun, X. Hu, H. Zhang, S. Zhang, Conversion and transformation of N species during pyrolysis of wood-

based panels: A review, Environ Pollut 270 (2021), 116120, https://doi.org/10.1016/j.envpol.2020.116120.

[55] Q. Ren, C. Zhao, Evolution of fuel-N in gas phase during biomass pyrolysis, Renew. Sustain. Energy Rev. 50 (2015) 408–418, https://doi.org/10.1016/j.rser.2015.05.043.

[56] N. Gil-Lalaguna, Z. Afailal, M. Aznar, I. Fonts, Exploring the sustainable production of ammonia by recycling N and H in biological residues: Evolution of fuel-N during glutamic acid gasification, J. Cleaner Prod. 282 (2021), 124417, https://doi.org/10.1016/j.jclepro.2020.124417.

[57] H. Nan, Z. Xiao, L. Zhao, F. Yang, H. Xu, X. Xu, H. Qiu, Nitrogen Transformation during Pyrolysis of Various N-Containing Biowastes with Participation of Mineral Calcium, ACS Sustainable Chem. Eng. 8 (32) (2020) 12197–12207, https://doi.org/10.1021/acssuschemeng.0c03773.